Astron. Astrophys. 324, 690–698 (1997)

ASTRONOMY
AND
ASTROPHYSICS

X-ray emitting stars in the NGC 1333 star forming region

Thomas Preibisch

Astronomisches Institut der Universität Würzburg, Am Hubland, D-97074 Würzburg, Germany (preib@astro.uni-wuerzburg.de)

Received 15 October 1996 / Accepted 11 February 1997

Abstract. We present the results of a very deep ROSAT HRI X-ray observation of the highly active star forming region NGC 1333. In total we could detect 20 X-ray sources, 16 of which we assume to be members to the cluster of pre main sequence stars. Since most of the stars in NGC 1333 are still deeply embedded in the molecular cloud ($A_V \lesssim 5 - 30$ mag), we use near infrared data to estimate individual extinctions for the calculation of X-ray luminosities.

One of the X-ray sources is identified with the optically invisible, very deeply embedded ($A_V \approx 28$ mag) infrared class I source SVS16, for which we find an extremely high X-ray luminosity of 2.8×10^{32} erg/sec, making this object one of the most X-ray luminous pre main sequence stars known to date.

Since we have already performed similar sensitive ROSAT observations of the young cluster IC 348 (the second active star forming region in the Perseus molecular cloud complex), we compare the X-ray properties of the young stars in NGC 1333 to those in IC 348. We find no evidence for a significant change of the X-ray luminosity function during the first few million years in the life of the pre main sequence stars.

Key words: X-rays: stars – open clusters: individual: NGC 1333 – stars: coronal – pre-main-sequence stars

1. Introduction

NGC 1333 is an optical reflection nebula within a highly active star forming region in the Perseus molecular cloud complex at a distance of 350 pc (Herbig & Jones 1983). The reflection nebula is illuminated mainly by the B9 star BD +30°549 (the brightest star at the upper left edge in Fig. 1) and the heavily reddened star SVS3 (Strom et al. 1976). The bright star BD +30°547 (in the lower part of Fig. 1) is probably a foreground object (cf. Cernis 1990).

The region south of BD +30°549, covering a field of about $20' \times 20'$, contains a massive core of dense molecular gas (Lada et al. 1974) and many signposts of low mass star formation, including Herbig-Haro objects, molecular outflows, jets, pre main sequence (PMS) stars, and infrared sources (e.g. Strom et al. 1976; Hodapp & Ladd 1995).

NGC 1333 has been the target of considerable observational effort: Herbig & Jones (1983) have determined relative proper motions for several Herbig-Haro objects and more than 70 stars in and near NGC 1333. R band and Hα observations have been performed by Strom et al. (1986). Cernis (1990) investigated the interstellar extinction in the vicinity of NGC 1333. Warin et al. (1996) performed CO observations and found evidence for ongoing shock driven star formation. Hodapp & Ladd (1995) studied the molecular hydrogen emission from the numerous bipolar jets in NGC 1333. Bally et al. (1996) recently discovered over 20 groups of new Herbig-Haro objects in the NGC 1333 region and take this as evidence for a nearly coeval microburst of star formation.

Several far infrared sources within the NGC 1333 region are listed in the IRAS Point Source Catalog. Harvey et al. (1984) and Jennings et al. (1987) performed more sensitive far infrared surveys and detected a number of compact dust cores. In some of these cores, especially in IRAS1 (see Knee et al. 1990), IRAS2 (see Ward-Thompson et al. 1996), and IRAS4 (see Sandell et al. 1991), candidates for protostellar sources have been found.

Since most stars in NGC 1333 are heavily reddened and the region contains many deeply embedded stars, near infrared (NIR) observations have played a crucial role in the study of this region. Strom et al. (1976) first mapped NGC 1333 in the NIR and discovered 25 sources. Aspin et al. (1994; ASR) performed a rather deep J, H, K band survey of a 100 square arcminutes region south of the optical reflection nebula and detected 134 stars with $K < 18$. The sensitivity of their survey was high enough to detect all cluster members (even $0.08 M_\odot$ PMS stars with extinctions of up to $A_V \approx 30$ are above their detection threshold), but the field covered in their study was only a relatively small fraction of the star forming region.

Recently, Lada et al. (1996; LAL) performed a NIR survey of the complete region. In their 432 square arcminutes field they discovered 275 stars with $K < 14.5$. They found that half of these stars are contained within two subclusters separated by about $5'$. The extinction of the stars in NGC 1333 has a mean value of $A_V \approx 7$ but shows a considerable spread up to $A_V \approx 30$. By modeling the infrared luminosity evolution, LAL estimated the age of the cluster to be no more than 10^6 years.

The motivation for our ROSAT study was twofold: first, it is very interesting to investigate one of the most active nearby

star forming regions in X-rays, especially since the X-rays allow a considerably deeper look through the molecular gas towards the embedded young stars than optical observations. Second, we have already performed a comparable sensitive X-ray study of the young cluster IC 348 (Preibisch et al. 1996), which is the other center of star formation activity in the Perseus molecular cloud complex. IC 348 has been studied in the NIR by Lada & Lada (1995; LL), and LAL performed a detailed comparison of IC 348 and NGC 1333. They found that both clusters are similar in many respects and characterized by essentially the same star formation rate. However, while in IC 348 star formation has been going on since about 6×10^6 years, the PMS stars in NGC 1333 are considerably younger. The comparison of these clusters therefore allows one to study two embedded clusters in very different stages of evolution.

2. X-ray observation and data analysis

We have observed the NGC 1333 region with the HRI detector onboard the ROSAT satellite. This instrument has a very good spatial resolution of about $3''$ (FWHM) but no energy resolution. The field of view is about $40' \times 40'$. A detailed description of ROSAT and the HRI can be found in Trümper et al. (1991) and David et al. (1993).

Our observation was split into two major parts. The first part was performed on 3 March 1995 with an exposure time of 4810 sec, the second part between 20 and 25 August 1995 with an exposure time of 35 850 sec. Before analyzing the data we merged both observation parts, yielding a total exposure time of 40 660 sec.

During the second part of our observation a hot spot appeared on the detector, resulting in a strong feature close to the edge of the field of view. This hot spot is thought to be a defect in a single pore of the micro channel plate (see MPE ROSAT Newsletter 42) that produces virtual count rates of up to 25 counts/sec. Fortunately, the hot spot is very well localized and remains fixed close to the edge of the detector. In our observation it influenced only a small region ($\approx 1' \times 2'$) rather far ($19'$) away from the center of our image. Since the hot spot has no effect on other parts of the image, we ignored this region in our subsequent analysis.

We performed a detailed data analysis with the EXSAS software system (cf. Zimmermann et al. 1993), which gave very good agreement with the results of the standard pipeline data analysis SASS.

2.1. Source detection and identification

The source detection was done by first performing the usual "sliding-window" technique implemented in EXSAS, what resulted in a list of possible source positions. Then each of these possible sources was investigated in detail with a maximum likelihood method, which compared the observed distribution of counts to a model of the point spread function and the local background (cf. Cruddace et al. 1988). The procedure calculated the probability of the null hypothesis P_0 that the observed distribution of counts is only due to a statistical background fluctuation. The "likelihood of existence" $\mathscr{L} = -\ln(P_0)$ provides a maximum likelihood measure for the presence of a source above the local background. We accepted all possible sources with $\mathscr{L} \geq 10$ (corresponding to a 4.8σ detection) as real. Finally, for all accepted sources the most likely values for the position of the source and the positional uncertainties were determined. A visual inspection of the image showed good agreement with the results of the source detection procedure.

In total, we could detect 20 X-ray sources in the image. The positions of the sources are given in Table 1. As can be seen by comparing the X-ray source positions with optical and infrared images (Fig. 1), all X-ray sources can be identified with either an optically visible star or a NIR source (see Fig. 1). To check the accuracy of the positions and to look for possible boresight errors in the ROSAT aspect system which might cause systematical errors in the source coordinates, we compared the X-ray positions with the known positions of the optical counterparts. For 13 sources we could use the optical positions from the study of Herbig & Jones (1983), for additional 4 sources we used optical positions from the *HST Guide Star Catalog* (Lasker et al. 1990). While we did not find any systematic deviation in declination, a slight but obvious systematic shift of about $4''$ was found in right ascension. After correcting the X-ray positions accordingly, the remaining deviations were mostly within $\pm 2''$, in good agreement with the intrinsic uncertainties of the X-ray source positions (see Table 1).

There is only one source for which the identification might be dubious: X13 is located between the infrared source SVS13 and star No 2 in ASR. Since the offset of the (corrected) X-ray position is $9''$ for SVS13 but only $3''$ for ASR–2, we prefer the identification with ASR–2. For all other sources there is only a single unique counterpart within the 3σ error circle and thus we conclude that the (corrected) X-ray positions and our identifications are very reliable.

We also checked whether our detection threshold of $\mathscr{L} \geq 10$ for accepting sources as real might be too conservative, especially since in other studies somewhat lower limits (e.g. $\mathscr{L} \geq 8$) have been used. This check was performed by looking for NIR counterparts of the possible sources. As pointed out by Casanova et al. (1995), the extinction of interstellar matter is very similar for the 1 keV ROSAT band and the NIR J band. In their ROSAT study of the embedded stars in the ρ Ophiuchi cloud core Casanova et al. (1995) found a good correlation between the X-ray count rate and the J magnitude. Our data show a very similar relation. Reducing the detection threshold to $\mathscr{L} \geq 8$ resulted in a few additional sources with count rates between 0.3 and 0.5 counts/ksec. For the NIR counterparts of these sources we would expect J magnitudes around $J \approx 13 \pm 2$ and thus they should have been easily detected by ASR, who had a 5σ limiting magnitude of $J_{\rm lim} \approx 20$. However, none of the additional sources in the region studied by ASR has a NIR counterpart within its error circle. Thus we conclude that these possible sources are most probably spurious detections and that our sample of X-ray sources with $\mathscr{L} \geq 10$ is the complete sample of sources detectable in our data.

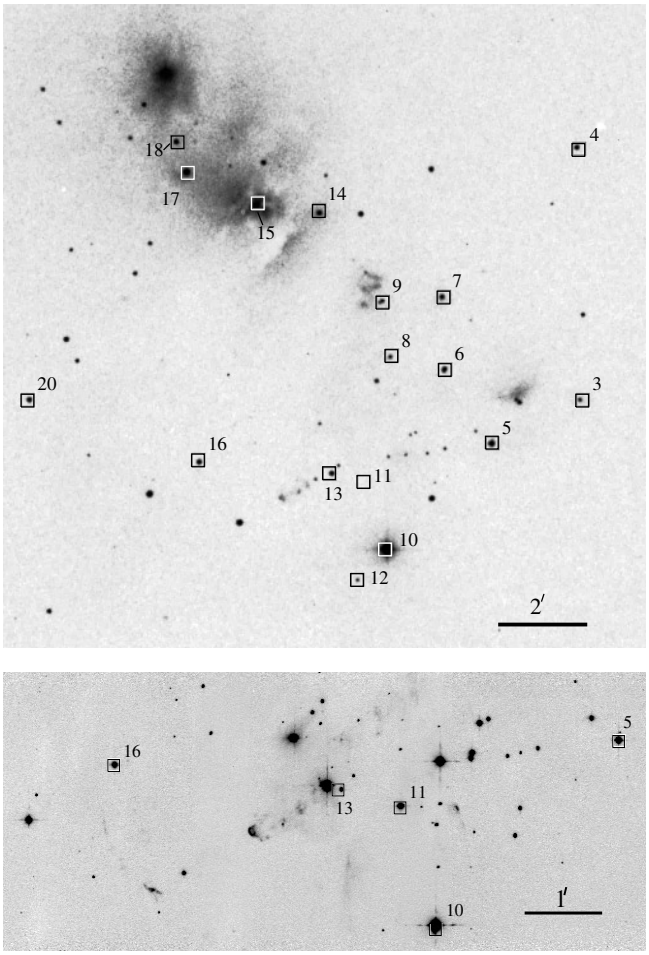

Fig. 1. Upper image: Optical image (produced from the Digitized Sky Survey) of a $15' \times 15'$ field in the NGC 1333 region. The positions of the X-ray sources are marked by the squares. Lower image: K-band image of the southern part of NGC 1333 from Hodapp (1994). The field of view is about $6.5' \times 3'$, the positions of the X-ray sources are marked by the squares.

2.2. Determination of count rates

In order to determine the count rates we choose circular source regions centered on the individual sources which were large enough to contain at least 99% of the counts according to the analytic model of the HRI point spread function implemented in EXSAS. As background regions we used concentric annuli with inner radius of 3 times and outer radius of 4 times the radius of the corresponding source regions. For some sources we had to evaluate the background from other nearby source free regions in order to avoid an overlap between the background region and the source region of another nearby source. To calculate the source count rates we determined the number of counts detected in each source and background region, corrected for vignetting and deadtime-effects and subtracted the scaled background counts from the source counts. The source count rates are given in Table 1.

Table 1. Positions, positional errors Δ, likelihood of existence $\mathscr{L}$, and count rate cr for the X-ray sources detected in the HRI observation. '1σ' errors are given for the uncertainties of the positions and count rates.

X	α(2000)	δ(2000)	Δ	$\mathscr{L}$	cr	$\pm$
	$3^h\ ^m\ ^s$	$31^\circ\ '\ ''$	[$''$]		[cnts/ksec]	
1	27 42.6	17 17	5	27.6	3.2	1.0
2	28 11.0	13 53	3	24.5	1.4	0.5
3	28 36.7	17 36	3	25.7	1.1	0.3
4	28 37.0	23 12	3	40.9	1.3	0.4
5	28 46.1	16 37	2	59.9	1.3	0.2
6	28 50.9	18 17	3	16.6	0.7	0.2
7	28 51.1	19 54	2	33.3	0.8	0.2
8	28 56.5	18 35	2	10.5	0.4	0.2
9	28 57.1	19 47	3	10.0	0.5	0.2
10	28 57.2	14 17	2	1424.7	12.7	0.6
11	28 59.4	15 47	2	32.4	0.8	0.2
12	29 00.1	13 35	3	12.4	0.4	0.2
13	29 03.0	16 01	2	15.7	0.5	0.2
14	29 03.7	21 50	3	19.5	0.9	0.3
15	29 10.4	22 00	2	163.8	3.0	0.4
16	29 16.7	16 19	2	18.3	0.5	0.2
17	29 17.7	22 46	2	459.9	6.0	0.5
18	29 18.7	23 26	2	115.0	2.4	0.3
19	29 26.7	26 48	3	84.7	4.2	0.8
20	29 34.4	17 43	2	84.9	1.9	0.4

We determined count rate upper limits for some well known PMS stars not detected as X-ray sources by comparing the counts in a detection cell at the target position with that of several nearby background regions. Then 90% confidence upper limits were computed by a Bayesian method described by Kraft et al. (1991)[1].

3. Membership

An important question to address is which of the X-ray sources actually are associated with the NGC 1333 star forming region and which are foreground or background sources. Our membership classification is based on four criteria. First, we investigate the X-ray source position relative to the densest parts of the NIR cluster. Second, we compare the proper motion of the optical counterparts of the X-ray sources to the mean cluster proper motion. Third, we look at the position of the stars in the HR diagram and check whether it is consistent with a PMS star at a distance of 350 pc (see Sect. 4.1). Finally, we note that the detection of strong X-ray emission is per se an indicator for the PMS nature of a star, since most PMS stars show $100 - 1000$ times higher X-ray luminosities than typical for main sequence stars (cf. Pallavicini 1989). In the following we use the first three criteria to find out which of the X-ray sources are probably not members of the NGC 1333 cluster.

[1] We note that the statistical basis of this method has been criticized in Feigelson & Babu (1992). It is nevertheless well suited for the purpose here.

Table 2. Identification and properties of the X-ray sources and some known PMS stars (from Herbig & Bell 1988) not detected as X-ray sources. SVS: number in Strom et al. 1976; ASR: number in ASR; HJ: number in Herbig & Jones (1983); $\mu_{\rm rel}$: proper motion relative to the cluster mean from Herbig & Jones (1983); V: visual magnitude; $W(\mathrm{H}\alpha)$: from Herbig & Bell (1988), otherwise a qualitative estimate of the emission line strength from Strom et al. (1986); NIRe: presence of a NIR excess; memb.: membership classification. The uncertainty of $\log L_{\rm X}$ is about 0.3 dex.

X	Name	SVS	ASR	HJ	$\mu_{\rm rel}$	V	$W(\mathrm{H}\alpha)$	NIRe	memb.	$A_{V,\rm IR}$	$L_{\rm bol,IR}$	$\log L_{\rm X}$	$\log\left(\frac{L_{\rm X}}{L_{\rm bol}}\right)$
		#	#	#		[mag]	[Å]			[mag]	[$L_\odot$]	[erg/sec]	
1	GSC 2342145					14.79			no				
2									no				
3				28	0.6				yes	9.2	4.6	31.2	-3.1
4				110	1.5				no(?)	1.7			-3.3
5	LkHα 351	21	128	30	0.2	15.57	m		yes	4.0	3.5	30.5	-3.6
6	LkHα 352a	10	122				s	yes	yes	4.9	1.9	30.4	-3.4
7			125	9	0.4		-	yes	yes	2.7	1.0	30.1	-3.4
8	SVS11	11	120	21	0.2		s	yes	yes	7.7	1.6	30.4	-3.4
9			115	19	0.2		m	yes	yes	0.8	0.4	29.6	-3.6
10	BD+30°547	19	130			9.68		yes	no	0.7*	6.1*	30.4	-4.0
11	SVS16	16	106					yes	yes	27.6	7.8	32.4	-2.0
12			51	4	0.4				yes	4.1	0.4	30.1	-3.0
13			2	6	0.3		m		yes	0.0	0.1	29.3	-3.2
14	SVS8	8		11	0.6			yes	yes	3.7	1.7	30.3	-3.5
15	GSC 2342359	3				12.28		yes	yes	2.9	9.7	30.7	-3.8
16			121	3	0.1		m		yes	2.6	1.4	29.9	-3.8
17	LkHα 270	2		103	1.0	14.23	31	yes	yes	0.5	3.4	30.5	-3.6
18	GSC 2342441			102	0.6	15.05			yes	0.1	0.3	30.0	-3.0
19	GSC 2342571	6				14.67			yes	4.1	3.7	31.1	-3.1
20				51	0.1				yes	2.1	0.7	30.4	-3.1
–	LkHα 271	20	123			14.7	186		yes	11.1	8.8	< 30.9	< -3.6
–	CoKu 1333/3		126			17.7	13	yes	yes	9.5	1.5	< 30.8	< -2.9
–	CoKu 1333/4		127			18.6	14	yes	yes	1.8	0.7	< 29.6	< -3.7
–	BD +30°549					10.47			yes	2.7**	100**	< 29.8	< -5.7

*: Calculated for the distance, spectral type, and extinction given by Cernis (1990).
**: Calculated for the extinction of A_V = 2.71 given by Cernis (1990) and an assumed distance of 350 pc.

First, we note that X1 and X2 are located in the outer parts our image and thus are probably not related to the star forming region. Furthermore, BD +30°547 = X10 is already known to be a foreground star. If we use the parameters given by Cernis (1990), V = 9.89, A_V = 0.69, spectral type G2IV, and distance 192 pc, we derive a bolometric luminosity of about $6L_\odot$, suggesting this star to be a $\approx 5 \times 10^6$ years old PMS star, perhaps related to the nearby Taurus Auriga molecular cloud complex. We therefore assume X1, X2, and X10 to be non-members of NGC 1333.

As can be seen in Fig. 2, the other X-ray sources are strongly concentrated towards the densest regions of the NIR cluster found by LAL, suggesting that most of them are associated to the cluster. Further evidence for membership comes from the proper motions measurements of Herbig & Jones (1983): For 13 of the remaining X-ray sources proper motions are known and, with the only exception of X4, are consistent with cluster membership, based on the criterion that the stars proper motion relative to the mean motion of the cluster members is $\mu_{\rm rel} \leqq 1$ (see Table 2). We therefore assume X4 to be probably no member of the star forming region but a foreground star.

Thus we conclude that the sources X1, X2, X4, and X10 are probably not related to the NGC 1333 star forming region, but the remaining 16 X-ray sources are members to this region. We do not believe that this sample of X-ray members is further contaminated by foreground or background sources for the following reasons:

Contamination due to background sources is improbable, because the large extinction in the molecular cloud should prevent background stars from shining through the cloud. It should be noted that with the only exception of X11 all X-ray sources have rather bright optical counterparts. The only background stars that might be visible through the molecular cloud with an extinction of $5 \leq A_V \lesssim 30$ are very bright giant stars or O

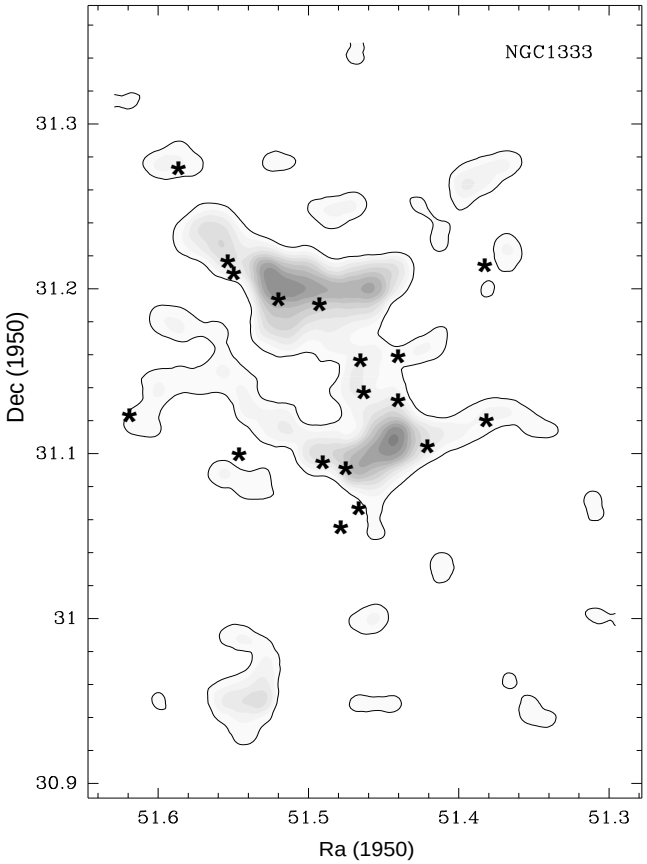

Fig. 2. Greyscale contour map of the surface density distribution of K band sources, adapted from Fig. 2b in LAL. The boundary of the lowest greyscale level, corresponding to a surface density of three times the average background/foreground field star density, is additionally shown as a solid contour line. The positions of the X-ray sources are marked by the asterisks.

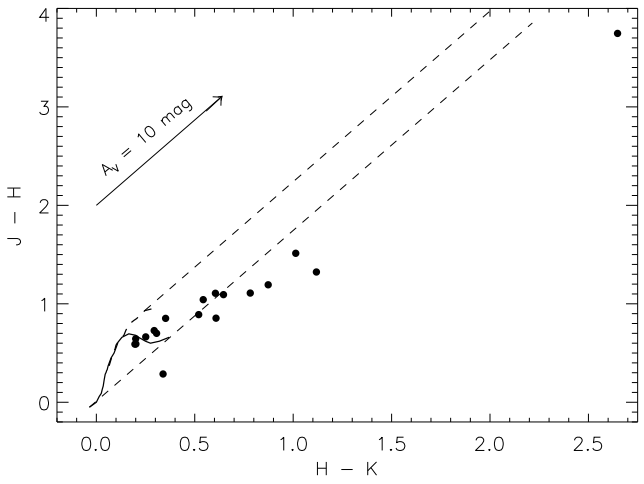

Fig. 3. NIR color-color diagram of the X-ray sources based on the NIR data from LAL. The thick solid line shows the main sequence, the thick dashed line the giant branch. The dashed lines show the reddening band for main sequence colors, the arrow shows the reddening vector for A_V = 10 mag. The object at $J-H \approx 0.3$, $H-K \approx 0.35$ is the foreground star BD +30°547 = X10.

type stars. However, the X-ray emission from O type stars is characterized by $L_{\rm X}/L_{\rm bol} \approx 10^{-7}$ (Pallavicini 1989; Cassinelli et al. 1994), and giant stars generally show $L_{\rm X}/L_{\rm bol} \lesssim 10^{-6}$ (Hünsch et al. 1996). This is several orders of magnitude lower than the ratios we find for the sources in NGC 1333 (see Table 2).

Since there are no early type foreground stars, the only foreground contamination to be expected is due to K and M dwarfs, among which the most active objects might have $L_{\rm X}/L_{\rm bol}$ ratios similar to that of the PMS stars (cf. Schmitt et al. 1995). The number of expected foreground sources can be estimated using the X-ray luminosity function of the K and M stars in the solar neighborhood as given in Schmitt et al. (1995). As shown in Randich et al. (1995), from a statistical method developed by Schmitt & Snowden (1990), a simple formula for the number of expected foreground sources as a function of the minimal detectable X-ray source flux and the solid angle of the region of interest can be derived (Eq. (5) in Randich et al. 1995). To apply this method to our HRI data, we estimate the minimal detectable X-ray flux from the count rates of the weakest sources to be $\approx 8 \times 10^{-15}$ erg/(sec cm^2). Thus, for the central $20' \times 20'$ region we derive a number of 1.4 expected foreground sources. This is in good agreement with the assumption of X4 being the only foreground object in our sample.

4. X-ray properties of the PMS stars

4.1. Extinction and bolometric luminosity of the X-ray sources

Most of the stars in NGC 1333 are deeply embedded in the molecular cloud, and thus we have to determine the individual extinction for each object in order to calculate the X-ray luminosity from the measured count rate. Since no detailed extinction determinations are available for most stars in our sample, we estimated the extinctions from the NIR colors of LAL, kindly provided to us by C. Lada and J. Alves. For 10 of our X-ray sources NIR colors were are also determined by ASR. In most cases the ASR data agree quite well with the LAL data within the uncertainties of $0.1-0.2$ mag. In order to perform a consistent analysis for all X-ray sources, we preferred the LAL data in all cases.

The position of the X-ray sources in the NIR color-color diagram is shown in Fig. 3. One can see that about half of the stars lie within the reddening band originating at normal main sequence colors, what indicates that the NIR colors are consistent with reddened photospheric emission. The other objects lie below the reddening band and thus show infrared excess emission probably caused by circumstellar matter.

In principle, it is not possible to fully disentangle the effects of reddening and excess emission, since both processes move the star in similar directions in the color-color diagram. Thus there is no unique way to deredden the stars and we have to make two simplifying assumptions: All stars with colors consistent with

those of reddened main-sequence stars are assumed to have no NIR excess and are dereddened by shifting them parallel to the reddening line down to the main sequence. All stars lying below the reddening line for M6 dwarfs are classified as NIR excess stars and dereddened by shifting them parallel to the reddening line to $(J-H)_0 = 0.8$, which was found by Strom et al. (1994) to be typical for classical T Tauri stars with NIR excesses. The length of the reddening path gives $E(J-H)$, and we used the relations $A_J = 2.64 \times E(J-H)$ (Greene et al. 1994) and $A_{V,\mathrm{IR}} = 3.55 \times A_J$ (Rieke & Lebofsky 1985) to estimate the visual extinction $A_{V,\mathrm{IR}}$. As shown by Greene et al. (1994), there is a good correlation between the bolometric luminosity and the dereddened J band flux. We used this correlation (Eq. (2) in Greene et al.) to estimate the bolometric luminosities $L_{\mathrm{bol,IR}}$ of the stars.

However, even with the simplifying assumptions mentioned above, there is no unique way to deredden stars within the reddening band. One can either deredden them towards the nearly horizontal branch of M0 to M6 dwarfs at $(J-H)_0 \approx 0.6$ or further down towards earlier spectral types. We solved this problem by tentatively trying both possibilities. This results in two different extinctions and also two different bolometric luminosities for each star. Furthermore, the intersections of the reddening path with the main sequence give two estimates for the spectral type. We can therefore draw two positions for each star into an HR diagram and compare them with the PMS evolutionary tracks of D'Antona & Mazzitelli (1994). For all stars within the reddening band, only one of the two reddening solutions results in a location between the stellar birthline and the main sequence, and thus is consistent with a PMS star at the distance of 350 pc. The other reddening solution either gives a location below the main sequence or above the birthline, what is clearly inappropriate for stars classified as cluster members. So this procedure provides us not only with a unique solution for the dereddening problem, but also shows that we can find a set of parameters $(A_{V,\mathrm{IR}}, L_{\mathrm{bol,IR}})$ consistent with the PMS nature of the stars. We are aware that this way of estimating a spectral type from the NIR colors is subject to rather large uncertainties and therefore we will not try to estimate stellar ages and masses from comparison with evolutionary tracks in the HR diagram.

The extinctions and bolometric luminosities are given in Table 2. In order to quantify the uncertainties of these values, we assume that the uncertainty in $E(J-H)$ is about ± 0.1, corresponding to an error of $\Delta A_{V,\mathrm{IR}} \approx \pm 1$ for stars within the reddening band. For NIR excess sources the estimated uncertainty in $E(J-H)$ is $\lesssim \pm 0.2$, resulting in $\Delta A_{V,\mathrm{IR}} \lesssim 2$. This causes uncertainties in the X-ray luminosities of $\Delta \log L_{\mathrm{X}} \lesssim 0.3$.

4.2. X-ray luminosities

In order to calculate the X-ray luminosities we interpreted the X-ray emission as optically thin thermal plasma emission (see Raymond & Smith 1977). For the calculation of the interstellar absorption of X-rays we used the relation $N_{\mathrm{H}} = A_V \times 1.8 \times 10^{21}\,\mathrm{cm}^{-2}$ (Paresce 1984; see also Predehl & Schmitt 1995), and the soft X-ray opacities of Morrison & McCammon (1983). We assumed a plasma temperature of $kT = 1$ keV, what is typical for stellar X-ray sources (cf. Schmitt et al. 1990) and also PMS stars (e.g. Preibisch et al. 1997). With these values for N_{H} and kT we computed model X-ray spectra and determined the transformation factors between count rate and *de*reddened X-ray flux by folding the model X-ray spectra through the detector response function with the corresponding EXSAS commands.

The resulting X-ray luminosities (computed for the ROSAT band of $0.1-2.4$ keV) and ratios $L_{\mathrm{X}}/L_{\mathrm{bol}}$ are given in Table 2. With the exception of X11 (see Sect. 5), the X-ray properties of the stars in NGC 1333 are quite similar to those of X-ray detected late type PMS stars in other star forming regions (cf. Feigelson et al. 1993; Gagné & Caillault 1994; Casanova et al. 1995; Preibisch et al. 1996).

4.3. X-ray variability

In order to investigate the variability of the X-ray sources, we extracted X-ray lightcurves. The lightcurves were binned into 1000 sec intervals and a Kolmogorov-Smirnov test for variability was performed. The null hypothesis of this test is that the source is constant and all count rate variations are only statistical fluctuations. For X1, X6, X11, and X16 the null hypothesis can be rejected at $P_0 \leq 0.05$, which means that these sources are variable with more than 95% probability. The lightcurves for these sources show only low-level variability with amplitudes not exceeding a factor of 2–3. No events like the large X-ray flares seen on some other PMS stars (e.g. Montmerle et al. 1983; Preibisch et al. 1993) were found.

5. The X-ray emission from the infrared source SVS16

Our X-ray source X11 deserves special attention. In the optical image (see Fig. 1) and also in the R and I images in ASR nothing is visible at the position of the X-ray source. However, in the K band image (see Fig. 1) we find a perfect identification with the rather strong infrared source SVS16, originally detected in the K band by Strom et al. (1976). SVS16 is extremely red, the reddest object in the color-color diagram shown in Fig. 3. From the NIR colors we find a very large extinction of $A_{V,\mathrm{IR}} \approx 28$ mag, suggesting this star to be a very deeply embedded object. This results in an extremely high X-ray luminosity of $L_{\mathrm{X}} = 2.8 \times 10^{32}$ erg/sec. It should be noted that the source did not show a large flare during our observation, so this is a quiescent X-ray luminosity.

Before accepting such an extremely high X-ray luminosity as real, we carefully have to exclude possible misinterpretations. Based on the high extinction, we certainly can exclude this source to be a foreground object. The optical and NIR data alone do not allow to fully rule out the possibility that it might be a background O type or giant star. However, if we tentatively assume it to be a background O star, the extinction determined from the NIR colors would be even higher, $A_{V,\mathrm{IR}} \approx 35$ mag, and we would find a ratio $\log\left(L_X/L_{\mathrm{bol}}\right) \approx -4.9$. This is much higher than the typical ratio for O stars: In a ROSAT study of 1838 OB stars Berghöfer

et al. (1996) found a typical ratio $\log\left(L_{\rm X}/L_{\rm bol}\right) \approx -7$ and all O stars showed $\log\left(L_{\rm X}/L_{\rm bol}\right) < -5.5$. Thus the X-ray properties of SVS16 strongly argue against the interpretation as a background object. Also, the background hypothesis would not explain the strong NIR excess.

Further evidence comes from the H_2 emission image of Hodapp & Ladd (1995). In this image, an Herbig-Haro object can be seen about 30″ north-west of SVS16 and another one about 50″ south-east of SVS16. They both show a bow shock structure which indicates SVS16 to be the source of the corresponding outflow. We therefore conclude that SVS16 is actually a PMS star deeply embedded in NGC 1333. From the K- and L-band magnitudes given in Strom et al. (1976) we can calculate the infrared spectral index a as defined by Wilking et al. (1989) and find a = 1.94. This indicates that SVS16 is a Class I source, i.e. a PMS star with a a dense circumstellar envelope in a very early stage of evolution. The X-ray luminosity of this object exceeds that of nearly all other late type PMS stars by at least one order of magnitude. There is only one comparable object known: the infrared source IRS43 in the ρ Ophiuchi cloud core, which also is a Class I source. IRS43 was detected in a deep ROSAT PSPC observation with $\log L_{\rm X}$ = 32.2 by Casanova et al. (1995) and recently a ROSAT HRI observation confirmed the identification of the X-ray source with IRS43 (Grosso et al. 1997).

While the typical X-ray luminosities of PMS stars ($\log L_{\rm X}$ = $29-31$) can be explained by enhanced solar like coronal activity (c.f. Montmerle et al. 1993), it seems questionable whether the extremely high X-ray luminosity we find for SVS16 might also be explained in this way. Due to the lack of further information about this object, it is hard to answer this question. All we can do at the moment is to perform an order of magnitude estimate for the X-ray surface flux by tentatively assuming a spectral type of K5 for SVS16. In that case the stellar radius estimated from the bolometric luminosity as given in Table 2 would be about 4.7 $R_\odot$ and we would find an X-ray surface flux of $F_{\rm X} \approx 2 \times 10^8$ erg/(cm^2 sec). This is close to the maximum of the observed distribution of X-ray surface fluxes of PMS stars and very active main sequence stars (see eg. Bouvier 1990; Preibisch 1996) and thus we cannot exclude a solar like coronal origin.

We have already initiated a program of observations to further investigate this very interesting object. The first results will be published in a forthcoming paper.

6. Comparison with IC 348

NGC 1333 and IC 348 are the two most active star forming regions in the Perseus molecular cloud complex. These two clusters share many similarities but at the same time are quite different. So it is very interesting to compare the X-ray properties of the stars in these clusters. The PMS stars in NGC 1333 and IC 348 are ideally suited for such a comparison: both clusters are at the same distance and have not only been studied in equal sensitive X-ray observations (for IC 348 see Preibisch et al. 1996), but also in equal sensitive NIR observations (LL for IC 348, LAL for NGC 1333).

LL and LAL performed a detailed comparison of the NIR data and modeled the K band luminosity functions of both clusters. Their results can be summarized as follows: Both clusters are forming out of a molecular cloud core that originally contained a total gas and dust mass of about 500 $M_\odot$ with a very similar star formation rate of about 4×10^{-5} $M_\odot$ yr^{-1}. The differences between the clusters can be explained by the fact that in IC 348 star formation seems to be going on since about 6×10^6 years, while in NGC 1333 it started at most 10^6 years ago. This is the reason why IC 348 contains a dense cluster of several hundred stars, whereas in NGC 1333 not much more than 100 stars have formed up to now. NGC 1333 might become very similar to IC 348 if star formation were to continue for another $\approx 5 \times 10^6$ years. So NGC 1333 is a good proxy for the young IC 348.

The much earlier stage of evolution of NGC 1333 as compared to IC 348 can also be inferred from signposts of star forming activity. For example, jets and outflows have a very short dynamical timescale (typically $\lesssim 10^5$ years) and therefore are good indicators of extremely early stages of star formation. While in IC 348 only a single molecular hydrogen jet is known (HH211; see McCaughrean et al. 1994), NGC 1333 contains a large number of outflows and jets (Hodapp & Ladd 1995; Bally et al. 1996). Furthermore, most stars in NGC 1333 are still considerably deeper embedded in the molecular cloud than those in IC 348 and more than 60% of the NGC 1333 stars show NIR excesses (LAL), while in IC 348 this fraction is only about 20% (LL).

In order to investigate whether the X-ray properties of the stars in NGC 1333 are different from those of the considerably older stars in IC 348, we will compare the X-ray luminosity functions of the late type (F0 – M5) stars. For a meaningful comparison, we have to take into account that we could detect only a fraction of all cluster members in our X-ray observations. This means that we have to derive upper limits for the X-ray luminosities of the undetected cluster members.

The sample for NGC 1333 is constructed in the following way: We start from the 75 objects within the NIR double cluster for which LAL could determine the NIR colors (see Fig. 4 in LAL). Since about 5 foreground or background sources are expected in this area, there are about 70 members. 16 of these 70 members were detected in our X-ray observation, for additional 3 members we could derive individual upper limits (see Table 2; BD +30°549 is excluded because it is an early type star). Since no detailed membership information is available for the other NIR sources, we simulate the upper limits for the X-ray undetected cluster members in the following way: We assume these stars to have a distribution of extinctions as found from the NIR colors of the stars in Fig. 4 in LAL. We use these extinctions and a count rate upper limit of 0.3 counts/ksec to calculate upper limits for the X-ray luminosities. In order to derive the X-ray luminosity function for this sample with 16 detections and 54

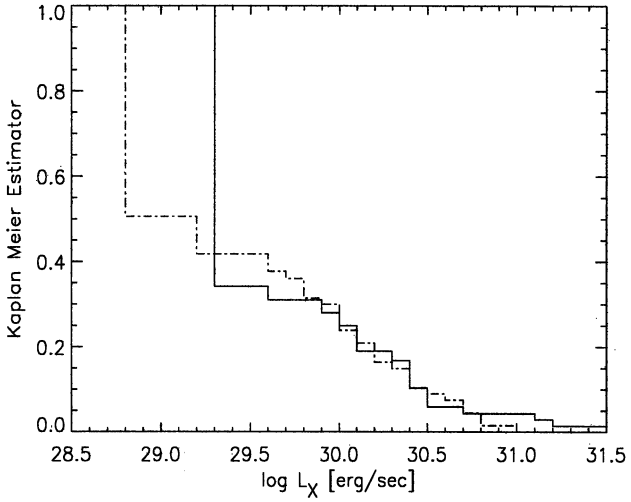

Fig. 4. Comparison of the Kaplan Meier Estimator for the cumulative X-ray luminosity functions of NGC 1333 (solid line) and IC 348 (dashed-dotted line).

upper limits we calculate the Kaplan-Meier estimator[2] using the ASURV statistical software package (Feigelson & Nelson 1985; LaValley et al. 1992). The luminosity function for IC 348 is constructed in a similar way and based on the 67 members in the central $6.5' \times 6.5'$ region, among which 30 objects were detected as X-ray sources.

The luminosity functions are compared in Fig. 4. The luminosity function for IC 348 extends towards lower X-ray luminosities since the average extinction is smaller than in NGC 1333. Above $\log L_X \approx 29.5$, however, the luminosity functions are very similar. This visual impression is confirmed by the results of the Two-Sample Tests in ASURV. We find values between 0.63 and 0.83 for the probability of the null-hypothesis that both samples are drawn from the same distribution. This means that there is no significant difference in the X-ray luminosity functions of NGC 1333 and IC 348. The PMS stars in NGC 1333 thus have similar X-ray luminosities as the considerably older stars in IC 348 and we find no evidence for an evolution of the cluster X-ray luminosity function in the age period between 1 Myr and 6 Myrs.

This result is consistent with the assumption of a solar like coronal origin for the X-ray emission of the PMS stars. For coronal X-ray emission the most fundamental relation that determines the X-ray luminosity seems to be the relation between the stellar rotation rate and the X-ray surface flux. This means that the evolution of the X-ray luminosity is governed by the rotational evolution and the radius evolution of the PMS stars. For main sequence stars as well as PMS stars an increase of the X-ray surface flux with the rotation rate is well established (see e.g. Pallavicini et al. 1981; Bouvier 1990), however with some saturation effect occurring for very fast rotating stars ($P_{\rm rot} \lesssim 3$ days). During the PMS evolution between 1 Myr and 6 Myrs, stars have a tendency to spin up, but the change in rotation rate can be very different from star to star. For example, according to the model of Bouvier & Forestini (1994) for solar mass PMS stars, some stars might spin up by factors of up to 30 during this time, while others (which are magnetically coupled to their circumstellar disk) might not spin up at all (see also Fig. 5 in Bouvier et al. 1997). At the same time the PMS stars contract. For example, according to the D'Antona & Mazzitelli (1994) evolutionary tracks the surface area of a solar mass PMS star reduces by about a factor of 5 between 1 and 6 Myrs.

Taking everything together, there is an increase in rotation rate which probably leads to an increase in the X-ray surface flux but at the same time there is a decrease in the stellar surface area. So it depends on the details of these processes whether the X-ray luminosity of a specific star will increase, decrease, or be constant. It seems reasonable that for a sample of PMS stars the increase and decrease of the individual X-ray luminosities will approximately cancel and there is no significant net change in the X-ray luminosity function in the range of ages from 1 to 6 Myrs.

7. Summary and conclusions

In our deep ROSAT observation of the NGC 1333 star forming region we could detect X-ray emission from 16 PMS stars. With exception of X11, the X-ray luminosities and $L_X/L_{\rm bol}$ ratios we find are in the typical range found for X-ray detected PMS stars in other star forming regions. A comparison of the X-ray luminosity function of the sample of NIR cluster stars shows no significant difference to the X-ray luminosity function of the cluster IC 348, which is about 6 times older than NGC 1333. This is consistent with the assumption of enhanced solar like coronal activity as the origin of the X-ray emission from the PMS stars.

In the case of the X-ray source X11, that is identified with the optically invisible infrared source SVS16, however, a solar like coronal emission mechanism might have difficulties to explain the extremely high X-ray luminosity. Although the currently available data do not allow to exclude coronal X-ray emission, we would like to note that Hayashi et al. (1996) recently proposed an alternative model to explain the strong X-ray emission of very young PMS stars and protostars. They assume reconnection events in twisted magnetic field lines between the star and the circumstellar disk to heat the matter in huge magnetic loops up to very high temperatures ($\lesssim 10^8$ K), causing strong X-ray emission. There is increasing evidence, especially from ASCA observations, that PMS stars in the earliest stages of their evolution are strong sources of very hard ($\gtrsim 8$ keV) X-ray emission (e.g. Koyama et al. 1994, 1996). Although the Hayashi et al. model is highly speculative, it might be an interesting alternative to coronal X-ray emission.

Acknowledgements. I would like to thank Charles Lada and João Alves for interesting discussions and for providing me with their NIR data for the X-ray sources. I am grateful to the referee, Eric D. Feigelson, for his very constructive referee's report which helped to improve

[2] The Kaplan-Meier estimator is a maximum likelihood estimate for the cumulative distribution function of a censored sample (see Babu & Feigelson 1996).

this paper. This work was supported by the DARA under grant 05 OR 9103 0 and by the Deutsche Forschungsgemeinschaft through the Schwerpunkt Programm 'Physics of Star Formation' (grant Yo 5/18-1). The ROSAT project was supported by the Bundesministerium für Bildung, Wissenschaft, Forschung und Technologie (BMBF/DARA) and the Max-Planck-Society. The use of the Astrophysics Data System (ADS) provided by NASA, the SIMBAD database operated at CDS, and the Digitized Sky Survey provided by the Space Telescope Science Institute is acknowledged.

References

Aspin, C., Sandell, G., & Russel, A.P.G., 1994, A&AS 106, 165
Bally, J., Devine, D., & Reipurth, B., 1996, ApJ 473, L49
Babu, G.J. & Feigelson, E.D., 1996, *Astrostatistics*, Chapman & Hall, London
Berghöfer, T.W., Schmitt, J.H.M.M., Cassinelli, J.P., 1996, A&AS, 118, 48
Bouvier, J., 1990, AJ 99, 946
Bouvier, J. & Forestini, M., 1994, in "Circumstellar dust disk and planetary evolution", 10th IAP meeting, ed: Ferlet, p. 347
Bouvier, J., Wichmann, R., Grankin, K., et al., 1997, A&A 318, 495
Casanova, S., Montmerle, T., Feigelson, E.D., & André, P., 1995, ApJ 439, 752
Cassinelli, J.P., Cohen, D.H., MacFarlane, J.J., Sanders, W.T., & Welsh, B.J., 1994, ApJ 421, 705
Cernis, K., 1990, ApSS 166, 315
Cruddace, R.G., Hasinger, G.R., & Schmitt, J.H.M.M., 1988, in: *Astronomy from Large Databases*, eds. F. Murtagh & A. Heck, p. 177
D'Antona, F. & Mazzitelli, I., 1994, ApJS 90, 467
David, L.P., Harnden, F.R., Kearns, K.E., & Zombeck, M.V., 1993, *The ROSAT High Resolution Imager*, U.S. ROSAT Science Data Center/SAO
Feigelson, E.D. & Babu, G.J., 1992, *Statistical Challanges in Modern Astronomy*, Springer, p. 320
Feigelson, E.D. & Nelson, P.I., 1985, ApJ 293, 192
Feigelson, E.D., Casanova, S., Montmerle, T. & Guibert, J., 1993, ApJ 416, 623
Gagné, M., & Caillault, J.-P., 1994, ApJ 437, 361
Greene, T.P., Wilking, B.A., André, P., Young, E.T., & Lada, C.J., 1994, ApJ 434, 614
Grosso, N., Montmerk, T., Feigelson, E.D., et al., Nature 387, 56
Harvey, P.M., Wilking, B.A., & Joy, M., 1984, ApJ 278, 156
Hayashi, M.R., Shibata, K., & Matsumoto, R., 1996, ApJ 468, L37
Herbig, G.H. & Bell, K.R., 1988, Lick Observatory Bulletin No. 1111
Herbig, G.H. & Jones, B.F., 1983, AJ 88, 1040
Hodapp, K.-W., 1994, ApJS 94, 615
Hodapp, K.-W. & Ladd, E.F., 1995, ApJ 453, 715
Hünsch H., Schmitt J.H.M.M., Schröder K.-P., & Reimers D., 1996, A&A 310, 801
Jennings, R.E., Cameron, D.H.M., Cudlip, W., & Hirst, C.J., 1987, MNRAS 226, 461
Knee, L.B.G., Cameron, M., & Liseau, R., 1990, A&A 231, 419
Koyama, K., Maeda, Y., Ozaki, M., et al., 1994, PASJ 46, L125
Koyama, K., Hamaguchi, K., Ueno, S., Kobayashi, N., & Feigelson, E.D., 1996, PASJ, 48, L87
Kraft, R.P., Burrows, D.N. & Nousek, J.A., 1991, ApJ 374, 344
Lada, E.A. & Lada, C.J., 1995, AJ 109, 1682, (LL)
Lada, C.J., Gottlieb, C., Litvak, M., & Lilley, A.E., 1974, ApJ 194, 609
Lada, E.A., Alves, J., & Lada, C.J., 1996, AJ 111, 1964 (LAL)
Lasker, B.M., Sturch, C.R., McLean, B.J., et al., 1990, AJ 99, 2019
LaValley, M., Isobe, T., & Feigelson, E.D., 1992, BAAS 24, 839
McCaughrean, M.J., Rayner, J.T., & Zinnecker, H., 1994, ApJ 436, L189
Montmerle, T., Koch-Miramond, L., Falgarone, E., & Grindlay, J.E., 1983, ApJ 269, 182
Montmerle, T., Feigelson, E.D., Bouvier, J., & Andre, P., 1993, in: *Protostars and planets III*, eds. E.H. Levy & J.I. Lunine, University of Arizona Press, p. 689
Morrison, R. & McCammon, D., 1983, ApJ 270, 119
Pallavicini, R., 1989, A&A Rev. 1, 177
Pallavicini, R., Golub, L., Rosner, R., Vaiana, G.S., Ayres, T. & Linsky, J.L., 1981, ApJ 248, 279
Paresce, F., 1984, AJ 89, 1022
Predehl, P. & Schmitt, J.H.M.M., 1995, A&A 293, 889
Preibisch, Th., 1997, A&A 320, 525
Preibisch, Th., Zinnecker, H., & Schmitt, J.H.M.M., 1993, A&A 279, L33
Preibisch, Th., Zinnecker, H., & Herbig, G.H., 1996, A&A 310, 456
Randich, S., Schmitt, J.H.M.M., Prosser, C.F., & Stauffer, J.R., 1995, A&A 300, 134
Raymond, J.C. & Smith, B.W., 1977, ApJS 35, 419
Rieke, G.H. & Lebofsky, M.J., 1985, ApJ 288, 618
Sandell, G., Aspin, C., Duncan, W.D., Russel, A.P.G., & Robson, E.I., 1991, ApJ 376, L17
Schmitt, J.H.M.M. & Snowden, S.L., 1990, ApJ 361, 207
Schmitt, J.H.M.M., Collura, A., Sciortino, S., Vaiana, G.S., Harnden, F.R., & Rosner, R., 1990, ApJ, 365, 704
Schmitt, J.H.M.M., Fleming, T.A. & Giampapa, M.S., 1995, ApJ 450, 392
Strom, S.E., Vrba, F., & Strom, K.M., 1976, AJ 81, 314
Strom, K.M., Strom, S.E., Wolff, S.C., et al., 1986, ApJS 62, 39
Strom, K.M., Strom, S.E., & Merrill, K.M., 1994, ApJ 412, 233
Trümper, J. et al., 1991, Nature 349, 579
Ward-Thompson, D., Buckley, H.D., Greaves, J.S., Holland, W.S., & André, P., 1996, MNRAS 281, L53
Warin, S., Castets, A., Langer, W.D., Wilson, R.W., & Pagani, L., 1996, A&A 306, 935
Wilking, B.A., Lada, C.J., & Young, E.T., 1984, ApJ 340, 823
Zimmermann, H.U., Belloni, T., Izzo, C., Kahabka, P., & Schwentker, O., 1993, *EXSAS User's Guide*, MPE Report 244, Garching

This article was processed by the author using Springer-Verlag LaTeX A&A style file *L-AA* version 3.